Development of a new laboratory technique for high-temperature thermal emission spectroscopy of silicate melts

Rachel J. Lee,[1] Michael S. Ramsey,[1] and Penelope L. King[2]

Received 7 September 2012; revised 22 March 2013; accepted 15 April 2013.

[1] With the prevalence of glass and molten silicates in volcanic environments, and the important role of surface emissivity in thermal infrared (TIR) measurements, it is imperative to characterize accurately the spectral features associated with silicate glasses and melts. A microfurnace has been developed specifically for use with a laboratory Fourier transform infrared (FTIR) spectrometer to collect the first in situ TIR emission spectra of actively melting and cooling silicate glasses. The construction, implementation, and calibration of the microfurnace spectrometer system are presented here. Initial testing of the microfurnace is also discussed, which includes acquisition of thermal emission spectra of a quartz powder (unmelted), a melted and cooled oligoclase feldspar, and glassy melt of rhyolitic composition. Unlike a solid material, which may only have bending and stretching vibrations within its molecular structure, a fully molten material will exhibit several more degrees of freedom in structural movement, thus changing its spectral character. Differences in spectral behavior and morphology are observed between a glass in a solid state and its molten counterpart, confirming previous field measurements of lower emissivity upon melting. This laboratory microfurnace system has been designed to quantify the TIR emission spectral behavior of glassy materials in various physical states. Ultimately, it is hoped that the microfurnace data will help improve the ability of field-based, airborne, and spaceborne TIR data to characterize glassy volcanic terranes.

Citation: Lee, R. J., M. S. Ramsey, and P. L. King (2013), Development of a new laboratory technique for high-temperature thermal emission spectroscopy of silicate melts, *J. Geophys. Res. Solid Earth*, *118*, doi:10.1002/jgrb.50197.

1. Introduction

[2] Thermal emission spectroscopy and remote sensing have proven to be highly useful and practical techniques for nondestructive analysis of materials, particularly glassy structures [e.g., *Wyatt et al*., 2001; *Dalby et al*., 2006; *Dalby and King*, 2006; *Byrnes et al*., 2007; *Minitti et al*., 2007; *Dufresne et al*., 2009; *Lee et al*., 2010]. Vibrations of Si-O-Si and Al-O-Al (Si) bonds within silicate materials create prominent, unique, and identifiable absorption features in their thermal infrared (TIR) spectra [e.g., *King et al*., 2004, and references therein]. However, in comparison to their crystalline counterparts, TIR spectra of silicate glasses lack definitive features, and the Restrahlen feature tends to become broadened and muted [*Bell et al*., 1968; *Dowty*, 1987; *Crisp et al*., 1990; *Salisbury et al*., 1991; *Poe et al*., 1992a; *McMillan and Wolf*, 1995; *Agarwal and Tomozawa*, 1997; *McMillan et al*., 1998]. Furthermore, glass spectra are similar to one another regardless of composition, making accurate identification more difficult using TIR data, particularly at the lower spectral resolutions commonly encountered with remote sensing sensors. Despite this, high-resolution laboratory studies have shown that both the morphology and wavelength positions of silicate glass spectral features are dependent on wt.% SiO_2 content, Si-O bond distance, the presence and abundance of network modifying cations, and degree of polymerization [*Neuville and Mysen*, 1996; *Dalby et al*., 2006; *Byrnes et al*., 2007; *King et al*., 2008; *Dufresne et al*., 2009; *Lee et al*., 2010]. These past studies have focused on silicate glasses in a solid or quenched state. No prior laboratory studies exist that examine the thermal emission spectral characteristics of silicate glasses in a partially or fully molten state.

[3] However, the structural changes that occur in a glass as it undergoes melting have profound effects on thermal emission spectra, specifically the position, depth, and shape of the main absorption feature [e.g., *McMillan and Wolf*, 1995]. For example, studies of basalt flows using field-based TIR instrumentation have hinted that the broadband emissivity of molten basalt is significantly lower than that of its fully cooled counterpart [*Abtahi et al*., 2002; *Ramsey and Wessels*, 2007, *Ramsey et al*., 2012]. The energy emitted from a volcanic surface is particularly complex, variable, and commonly unpredictable. Lava flows and domes contain silicate materials with a range of temperatures, compositions, and vesicularities, as well as varying thicknesses of

[1]Department of Geology and Planetary Science, University of Pittsburgh, Pittsburgh, Pennsylvania, USA.
[2]Research School of Earth Sciences, The Australian National University, Canberra, Australia.

Corresponding author: R. J. Lee, Department of Geology and Planetary Science, 200 SRCC Bldg., University of Pittsburgh, Pittsburgh, PA 15260, USA. (rjl20@pitt.edu)

2169-9313/13/10.1002/jgrb.50197

glassy crust as they cool. Each of these factors combine in nonlinear ways to affect the spectral information derived from the surface [e.g., *Salisbury et al*., 1991; *Clark*, 1999; *Byrnes et al*., 2004; *Ramsey and Dehn*, 2004; *Vaughan et al*., 2005; *Wright and Ramsey*, 2006; *Carter et al*., 2007], and subtle changes in these material properties can indicate a change in the volcanic activity (e.g., extrusion rate, petrology, explosivity, etc.). Thus, the study of glassy and molten volcanic surfaces, and the ways in which they change over time, is also of great importance to volcanic hazard assessment and mitigation.

[4] A variety of spectroscopic techniques have been employed in the past to study the behavior of high-temperature and molten materials. Transmission and reflectance IR were used at a small scale to analyze glass samples heated to various temperatures [e.g., Grove *and Jellyman*, 1955; *Gervais and Piriou*, 1975; *Domine and Piriou*, 1983; *McMillan et al*., 1992; *Grzechnik and McMillan*, 1998]. The atomic absorption of a variety of gaseous and solid species was studied using vacuum graphite furnaces [e.g., *Woodriff and Ramelow*, 1968; *Brown et al*., 1973]. X-ray absorption spectroscopy and X-ray diffraction were used to assess changes in the structure of silicate glasses and melts [e.g., *Neuville et al*., 2004a, 2004b, 2008; *Farges and Brown*, 1996; *Ildefonse et al*., 1998; *Poe et al*., 2001; *Magnien et al*., 2004, 2006; *Sonneville et al*., 2012]. The presence and nature of magnetic phases in basaltic rocks heated up to 900 K was studied using Mossbauer spectroscopy [*Helgason et al*., 1994]. Raman spectroscopy was later used extensively in the study of the composition and molecular structure of aluminosilicate glasses and their corresponding melts [e.g., *Daniel et al*., 1995; *Mysen et al*., 1980, 1981, 1982; *Seifert et al*., 1981, 1982; *McMillan*, 1984; *Mysen*, 1988, 1990; *McMillan et al*., 1992, 1994; *Mysen and Frantz*, 1992, 1993; *Richet et al*., 1993; *Neuville and Mysen*, 1996; *Neuville et al*., 2004c, 2006; *Moulton et al*., 2012]. The local structure and bonding of aluminosilicate materials was investigated by nuclear magnetic resonance both below and above the glass transition temperature [e.g., *Kirkpatrick*, 1988; *Stebbins*, 1988; *Farnan and Stebbins*, 1990; *Stebbins and Farnan*, 1992; *Stebbins et al*., 1992; *Poe et al*., 1992b, 1993; *Stebbins and Xu*, 1997; *Gruener et al*., 2001], and these data were then compared to molecular dynamics simulations of the structure and relaxation of aluminosilicate liquids [e.g., *Poe et al*., 1994]. The complex nature of melt structure coupled with the challenge of performing in situ laboratory melting experiments at high temperatures (>1200°C) and small scales has, until now, precluded laboratory thermal emission spectral analysis of silicate melts.

[5] A microfurnace was constructed in order to perform in situ laboratory thermal emission analysis of silicate minerals, glasses, and melts. The design, construction, implementation, and calibration of the microfurnace are presented here. In addition, preliminary thermal emission spectra of quartz, oligoclase feldspar, and a well-characterized glassy melt of rhyolitic composition are discussed. With this new instrumentation and approach, the ways in which thermal emission spectra are affected by raising the temperature of silicate glasses through their glass transition and liquidus temperatures can now be more accurately understood. This work, along with low-temperature work [*Byrnes et al*., 2007; *Lee et al*., 2010], will help improve the ability of current TIR remote sensing data to accurately characterize volcanic glass composition and physical state, particularly in active volcanic environments. For example, TIR emissivity is an important parameter for accurate thermal models of lava flow development [e.g., *Baloga and Pieri*, 1986; *Crisp and Baloga*, 1990, 1994; *Harris et al*., 1998; *Harris and Rowland*, 2001; *Harris et al*., 2006; *Malin*, 1980; *Pieri and Baloga*, 1986; *Pieri et al*., 1990; *Vicari et al*., 2009], crust growth and lava rheology [e.g., *Keszthelyi and Denlinger*, 1996; *Anderson et al*., 1999], and the ability to map lava composition and texture [e.g., *Ondrusek et al*., 1993; *Ramsey and Fink*, 1996, 1997, 1999; *Byrnes et al*., 2000, 2004; *Ramsey and Dehn*, 2004]. Furthermore, the results can contribute to the design capabilities of future TIR remote sensing instrumentation.

2. Instrument Design

[6] The microfurnace was modeled after larger laboratory box furnaces, and the schematic design is shown in Figures 1 and 2. The heating elements are connected in series and are suspended downward into the furnace chamber, supported by alumina insulation. The unit is cylindrical in shape, and the inside is composed of nested cylinders of alumina insulating material. Samples are situated within a cylindrical tube, surrounded by the heating elements. This acts to focus radiation effectively from the heating elements onto the sample, making the microfurnace highly efficient for its size.

[7] In order to acquire emissivity spectra, the microfurnace chamber is opened via a small sliding door at the top. Emission from the sample is reflected into the spectrometer by way of a collimating mirror, which is situated directly above the sample port of the furnace. For safety, and because the microfurnace is in such close proximity to other temperature-sensitive equipment, it is vital to ensure that the top and sides of the unit never exceed 100°C. A water cooling system is incorporated into the design to regulate the exterior temperature. The heating elements, insulating material, water-cooling system, and power supply are all modular, which allows for simple removal and replacement of parts. Each component of the microfurnace is discussed below in detail.

2.1. Heating Elements

[8] In order to melt glass samples of dacite-rhyolite mineralogy, a maximum sample temperature of 1500°C is required, as determined by initial synthesis of a suite of synthetic glasses in this compositional range [*Byrnes et al*., 2007; *Lee et al*., 2010]. The heating elements within the microfurnace must be capable of reaching a temperature of approximately 1800°C in an oxidizing environment, allowing the target sample temperature to be achieved and also accounting for the expected heat losses due to conduction and convection. Molybdenum disilicide ($MoSi_2$) heating elements have a proven capability for use in industrial and laboratory sintering, heating, glass and metal melting operations, and thus have been used for this application.

[9] The microfurnace utilizes three Sentrotech 4/9 $MoSi_2$ heating elements with a shank length and hot zone of 7.6 cm. Each is rated at 300 W, providing up to 900 W of power. The microfurnace can reach a maximum temperature of 1500°C with the elements reaching ~1650°C–1700°C.

The heating elements are positioned around three sides of the furnace sample holder (Figure 3) and are connected in series with aluminum-nickel braided straps, using a custom mini bus bar system on the top of the microfurnace enclosure. The top 2 cm of the element shanks are aluminized to provide good contact with the power connections and can withstand temperatures up to 300°C. Each element is held in place using a custom alumina element holder that allows for easy element removal and replacement.

2.2. Power Supply and Temperature Control

[10] The $MoSi_2$ heating elements require a current and voltage of approximately 90 A at 14 V to reach an element temperature of 1700°C. An MHI Powerphase ST9001 single-phase silicon-controlled rectifier (SCR) power controller and an ACME T-1-13074 120V/16V 1500VA rated transformer are used to power the heating elements. This transformer is capable of delivering up to 100A at 16V. The SCR is equipped with variable output voltage, current limits, and a variable soft start to control the initial current to the heating elements, whose cold resistance is approximately one eighth of their hot resistance. The power output from the SCR is controlled by a 4–20 mA current signal.

[11] The power box, containing the SCR and transformer, is equipped with an ammeter, a voltmeter, and a small internal power supply with a 10-turn potentiometer to provide the 4–20 mA signal when used under manual control. Under automatic control, this signal is supplied by an Omega CN8201 single output proportional-integral-derivative (PID) temperature controller, with an RS232 connection to the laboratory computer for remote setup and monitoring. The input from a B-type (platinum-rhodium) thermocouple, located directly beneath the sample, is used along with the Omega controller to regulate the sample temperature. The controller can also be programmed to provide multistep ramp/soak recipes for the sample. The heating element temperature is monitored using an Omega DPi32 panel meter and an additional B-type thermocouple situated proximal to one of the heating elements. The power supply is connected to the microfurnace via two 120 A power cables. These cables, as well as the thermocouple and RS232 power cables, are shielded with braided metal cable to help minimize any electromagnetic interference with the internal components of the spectrometer.

2.3. Furnace Chamber

2.3.1. Insulation

[12] The cylindrical internal microfurnace chamber is composed of SALI alumina insulation from Zircar Ceramics. Alumina insulation is a widely used refractory insulation material in the furnace industry due to its high melting point (~2015°C), high strength, low density, and rigidity. It exhibits superior hot strength and stability at temperatures up to 1825°C, is nonreactive with most materials, undergoes minimal expansion upon heating, and can be easily cut into various shapes. The microfurnace consists of two nested 10.2 cm tall cylindrical pieces of SALI insulation, with notches cut out for the three heating elements (Figure 1a). These cylinders sit atop a circular, 2.5 cm thick SALI insulation base, which forms the "floor" of the microfurnace. Another 1.6 cm thick piece sits above the cylinders and supports the three heating element holders. A 3.8 cm hole in the center of the top piece houses the sample support post, and the three holes surrounding the sample support post allow for the hairpin heating elements to pass through to the center of the microfurnace (Figure 1a).

[13] The sample crucible support post consists of a 3.8 cm diameter, 1.3 cm thick dense alumina disk upon which the platinum sample crucible is situated. The disk has a pass-through hole for the sample temperature thermocouple. A 3.2 cm inner diameter, 3.5 cm long alumina furnace tube sits on the dense alumina disk and surrounds the sample crucible (Figure 1a). This entire assembly is supported from underneath by a 1 cm outer diameter, 0.6 cm inner diameter, 6.4 cm long alumina tube, which positions the sample support post at the necessary height to provide a 1 cm focused spot size emitting up to the mirror and into the spectrometer.

[14] All materials exposed to the spectrometer beam path when the microfurnace port is opened (e.g., the holders, furnace tube, sample support post, and surrounding insulation) are painted with cerium oxide high-temperature, high-emissivity paint. This paint is water-based, nonreactive, and noncorrosive. The coating helps prevent any spectral features of the alumina from contaminating the sample spectrum. This paint is one of the few cost-effective options for high-emissivity paint that can withstand very high operating temperatures and do so in an oxidizing environment, without reacting with any materials within the microfurnace.

[15] The sample chamber is covered with a 5.1 × 10.2 cm baffle (Figure 1b). This baffle is composed of Fractalin refractory alumina insulation and acts as a heat shield to protect the spectrometer and surrounding equipment from excess heat as the microfurnace heats to the desired temperature. When a spectrum is to be acquired, the user slides open the baffle and returns it to a closed position once the TIR emission spectrum has been collected. The baffle is also painted with cerium oxide in order to keep all internal surfaces of the microfurnace a consistent composition.

2.3.2. Sample Containment

[16] All samples are melted in custom-fabricated platinum crucibles within the microfurnace. Platinum is used because of the high melting point (~1770°C), stability at high temperatures, and the lack of oxidation or reaction with any of the surrounding materials or the sample. The crucibles are ~2.5 cm in diameter and hold up to 2 g of sample. Each is placed into and removed from the microfurnace using long platinum-tipped tongs. Once a cooled crucible is removed from the microfurnace, the sample is carefully removed. The crucible is then filled with sodium carbonate powder and placed into a muffle furnace at 900°C for ~20 min. The sodium carbonate acts to remove any glass residue from the platinum surface. The cooled sodium carbonate is removed from the crucible, and the crucible is placed into hydrochloric acid for several hours to dissolve any remaining material. This must be performed after each melt analysis in order to avoid contamination from one sample to the next.

2.3.3. Water Jacket

[17] In order to control the heat emitted from the microfurnace and protect surrounding equipment, a water cooling system surrounds the microfurnace on all sides (Figures 1a and 2). There are three components to the system: a bottom cooling plate, a cylindrical water jacket surrounding the furnace body, and a top cooling cover. Each of the components is independently sealed from one another

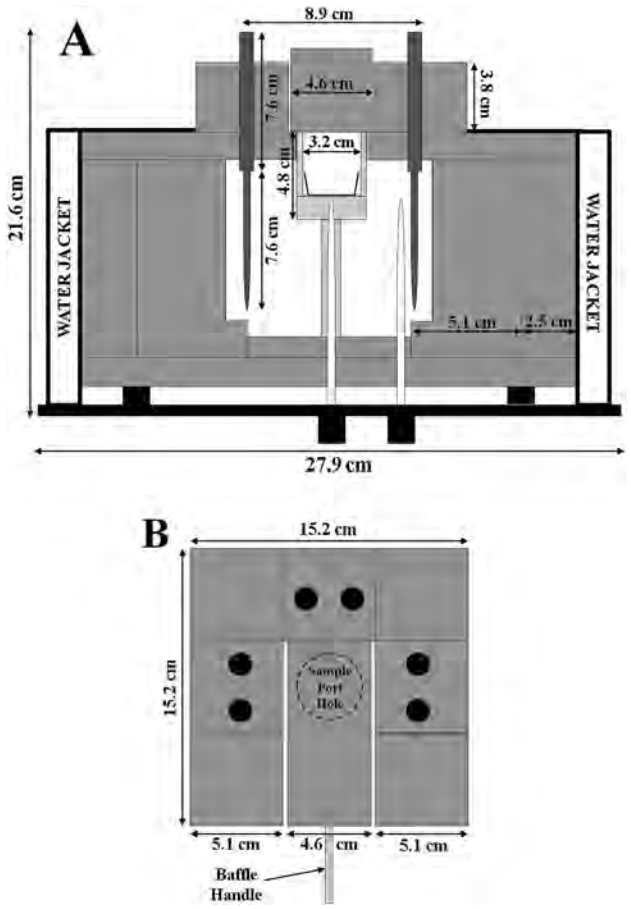

Figure 1. (a) Cross-sectional schematic of the microfurnace assembly, without the cooled cover in place. Medium gray-colored areas are insulation, heating elements are shown in dark gray, and the stainless steel shell and water jacket are shown in black. The dense alumina tube and sample support post (light gray) house the platinum crucible. The heating elements hang downward into air space inside the furnace and are connected to the power supply via a 2 cm section of shank above the heating element holders. (white tubes) Two B-type thermocouples measure the temperature of the sample and the heating elements and connect to the power supply through plugs at the bottom of the furnace. (b) Schematic view of the furnace looking down on the top, without the cooled cover in place. (black circles) The heating elements and their holders surround the sample port hole on three sides. The baffle covers the sample port hole during heating, and slides outward via the handle to expose the sample to the spectrometer for spectrum acquisition.

to avoid leaks. Additionally, the top cooling cover has a water-cooled baffle located directly over the alumina insulation baffle. When a sample spectrum is ready to be acquired, this water-cooled baffle slides aside, along with the alumina baffle. All three components have separate water-in/water-out spouts that are connected to one another and to the main water supply. The water temperature is maintained at ~25°C, and in order to prevent overpressurizing the system, a pressure regulator reduces the mains water pressure to <10 psi.

2.4. Spectrometer and Glove Box

[18] The microfurnace, standard "low-temperature" (80°C) spectrometer setup and all accompanying accessories are housed in a Plexiglas glove box adjacent to the external port of a Nicolet Nexus 670 Fourier transform infrared (FTIR) spectrometer (Figure 4). The standard setup equipment sits adjacent to the microfurnace on a sliding shuttle, which can be moved by the user from side to side to align the desired setup beneath the spectrometer mirror. The spectrometer and the glove box are both continuously purged using a Parker-Balston purge system, which reduces the TIR-active gases (CO_2 and H_2O) in the environment, thus maintaining a low relative humidity (<5%). The overall setup, spectral acquisition, and calibration follow that described by *Ruff et al*. [1997]. The glove box has several hand-ports that allow for access to all equipment within it without compromising the purged environment. This includes two sealable ports on the front for manipulating samples in the low-temperature setup and a port on the upper left that allows for operation of the microfurnace baffle. Each panel of the glove box is also fully removable, providing easy access to both setups for any needed maintenance or repair. The chamber is open to the external port of the spectrometer via a hole, which allows for the collimated emitted energy from the sample to pass into the spectrometer.

Figure 2. The microfurnace setup. The microfurnace is 21.6 cm in height and 28 cm in diameter at the base. The aluminum and stainless steel square cover on top of the furnace assembly, and the plastic and copper tubing, are part of the water cooling system. (white handle) The internal alumina baffle and the sliding portion of the top cover both move outward to expose the sample for analysis. Power is provided to the heating elements via the 120A black cables in the foreground.

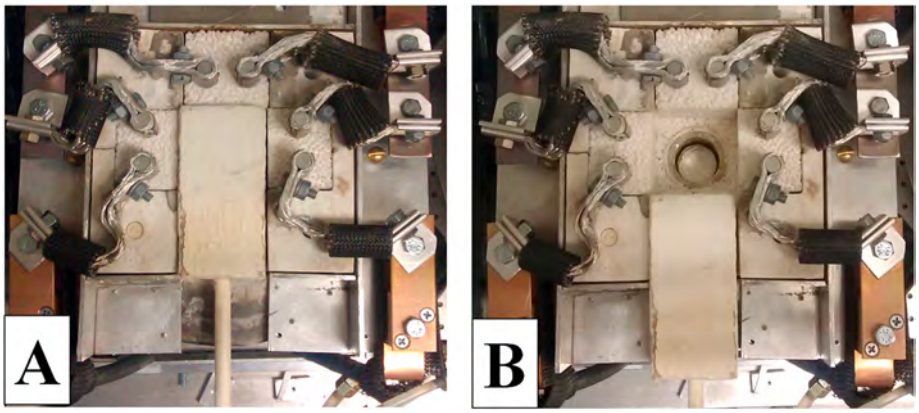

Figure 3. Three $MoSi_2$ heating elements surround the sample port on three sides. Heating elements are supported by alumina insulation and are connected to the power supply in series via insulated aluminum nickel braiding and a custom copper bus bar system. (black) Braids are covered with Insultherm insulation. (a) The alumina baffle covers the sample port hole during microfurnace heating. (b) When a spectrum is ready to be acquired, the baffle slides aside to reveal the sample.

3. Methodology

3.1. Initial Testing

[19] Prior to operating the microfurnace within the spectrometer setup, extensive testing was performed under a laboratory fume hood. The purpose of this testing was to study how the microfurnace operates and to determine any potential effects it may have on the surrounding laboratory environment. The air temperature above the open microfurnace port was measured to determine the height at which laboratory equipment and accessories can be safely situated above the furnace port. A K-type thermocouple was attached to the top cover of the microfurnace at the same position and height of the bottom of the mirror assembly. The mirror assembly has a maximum operating temperature of 200°C, and therefore air temperatures cannot exceed this temperature. The microfurnace was heated in 100°C increments from 500°C to 1200°C, and at each temperature, the port was opened for a 60 s time period. Temperature data from the thermocouple were digitally collected every 5 s using a Keithley multimeter.

[20] To test the efficacy of the water cooling system, the temperatures of the top and sides of the microfurnace were monitored using a tripod-mounted Forward Looking Infrared (FLIR) camera and a K-type thermocouple surface-mounted to the microfurnace exterior. The microfurnace was heated in 100°C increments from 500°C to 1500°C (sample temperature) and held at each temperature for 15 min. The FLIR camera acquired measurements every 10 min. The surface-mounted thermocouple was placed on the top cover near the port and monitored the change in surface temperature every 50°C as the microfurnace heated to temperature.

[21] In an effort to constrain the overall behavior of the heating elements, the element and sample temperature data were collected for an empty platinum crucible and for a quartz sand sample. These data served to document the behavior of the heating elements, the power controller, and the sample temperature as the microfurnace was heated to given temperatures over time. The difference between sample and element temperature was calculated for the empty crucible and quartz sand, and the overall behavior of this temperature difference was noted. If any problems arise in the future, these data can be reviewed to determine whether the heating elements, power supply, and other microfurnace components are performing as expected.

3.2. Sample Temperature

[22] In FTIR emission spectroscopy, measurements are converted into radiance via the instrument response function

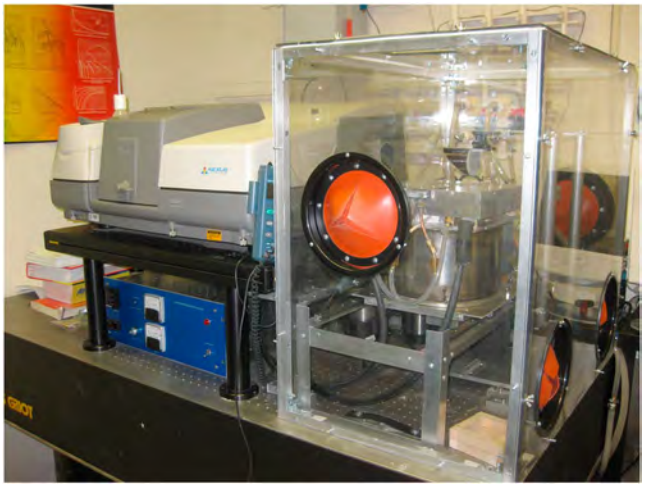

Figure 4. IVIS Laboratory spectrometer setup. The (left) Nicolet Nexus 670 FTIR spectrometer and (right) Plexiglas glove box sit atop a Melles Griot optical bench and are continuously purged of CO_2 and H_2O. Red silicone hand ports allow for access to the inside of the glove box for sample preparation and operation of the furnace baffle. The glove box is open to the external port of the spectrometer via a hole, which allows for the sample's emitted signal to pass into the spectrometer during acquisition. The power supply for the furnace sits beneath the spectrometer and is fully shielded to prevent electromagnetic interference with the spectrometer.

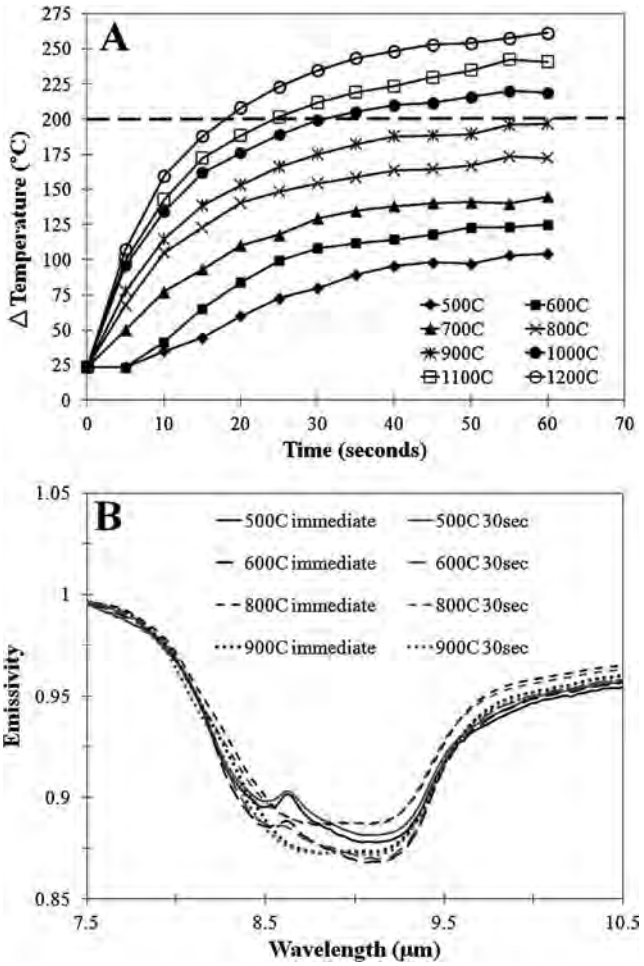

Figure 5. (a) The air temperature over the furnace port was tested during a 60 s time period at set points from 500°C to 1200°C. This was performed using a K-type thermocouples attached to the furnace port at the same height as the spectrometer mirror. At temperatures below 900°C, (shown by the dotted line) the air temperature does not exceed 200°C, which is the operating temperature limit of the mirror assembly. Over 1000°C, air temperature begins to rise above the 200°C temperature limit after 30 s. (b) Emissivity spectra of the quartz sample acquired immediately upon opening the furnace port versus spectra acquired 30 s after opening the port. For a given set point temperature, the change to spectral morphology and depth is minimal, indicating that the change in air temperature above the sample port has a minimal effect on the spectra.

[*Ruff et al*., 1997], which is the measure of the spectrometer's voltage output in response to input signal from the sample. For the standard low-temperature setup (e.g., sample temperature = 80°C), the response function is calculated by measuring the emissivity of a blackbody (emissivity = 1.0) at two different temperatures. The custom-designed blackbody is a 30° cone painted with high-emissivity blackbody paint and heated using wrap heating pads. The temperature of the blackbody is measured using two platinum resistance thermometers. These blackbody measurements are used to calculate the response function of the spectrometer and, ultimately, the emission spectrum of the sample. This "one-temperature" calibration for deriving emissivity is described in detail by *Ruff et al*. [1997], whereas the specific methodology used at the Image Visualization and Infrared Spectroscopy (IVIS) Laboratory at the University of Pittsburgh is described by *Byrnes et al*. [2007].

[23] For the microfurnace setup, direct temperature measurement of an independent blackbody and sample under the same conditions is not easily accomplished. The sample thermocouple beneath the platinum sample crucible measures the temperature of the crucible and serves as the assumed sample temperature. However, FLIR measurements of samples within the crucible show that the actual sample

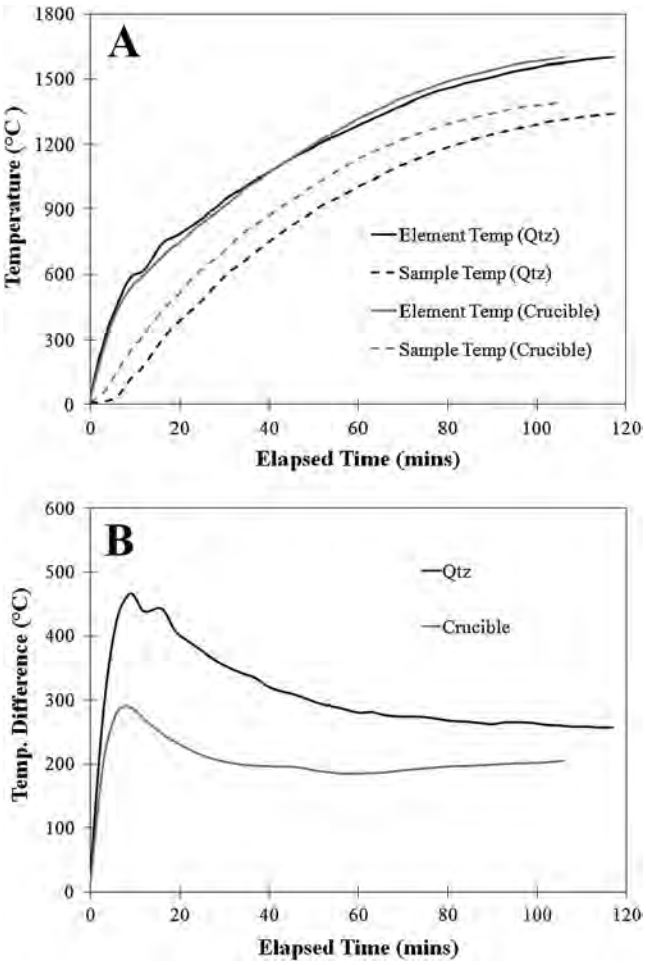

Figure 6. (a) Element temperature versus sample temperature for an (grey lines) empty Pt crucible and (black lines) a quartz sand sample. Element temperature remains virtually the same, as is expected; however, the quartz sand has a consistently larger temperature difference from the heating elements and also has a lower temperature than the platinum crucible. This can be attributed to a difference in thermal conductivity between the bare crucible and quartz sand. (b) The calculated difference between element and sample temperature over time. In both cases, the temperature difference is sharp as the heating elements initially heat up much faster than the sample. Eventually, the sample temperature stabilizes between ~200°C and 250°C lower than the heating elements.

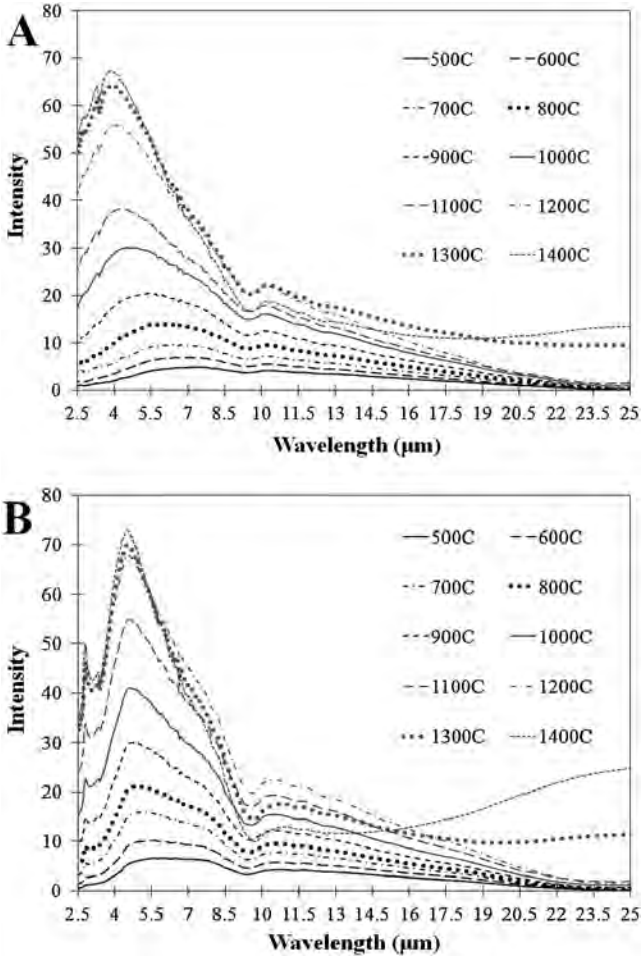

Figure 7. Intensity spectra for (a) cerium oxide pellets and (b) a glass sample contained in the platinum crucible. The sharp nonlinear behavior at longer wavelengths for temperatures greater than 1200°C is likely caused by the interaction of the large amount of energy with the spectrometer detector where the signal-to-noise ratio (SNR) is already low.

temperature can vary from that of the thermocouple, which suggests the temperature at the bottom of the crucible is somewhat hotter than that of the sample surface. The size of this difference is dependent upon sample type and furnace set point temperature. This temperature difference cannot be avoided in the current design and is likely introduced into the sample spectrum after the microfurnace is opened and the sample surface begins to cool with exposure to the air. The sample thermocouple and FLIR camera were therefore used together to assess the general behavior of sample temperature. At each set point, the microfurnace port was opened, and 10 FLIR images (one per second) were acquired of the sample within the crucible. During postprocessing of the FLIR data, a 1 cm diameter annotated circle was added to each FLIR image to approximate the spot size of the spectrometer. The average sample temperature within the circle was determined, and the 10 average sample temperature images were averaged for each set point. This provided an overall average sample temperature for the time over which the furnace port would likely be open for spectrum acquisition.

3.3. Calibration

[24] No material was found that behaves as a perfect blackbody across the entire temperature range of the microfurnace and also operates effectively at the high furnace temperatures. External blackbody standards, which go up to 2500°C, do exist but they are costly and would not accurately mimic the sample environment conditions, thus invalidating the one-temperature calibration approach [*Ruff et al.*, 1997].

[25] In addition to high-emissivity paint, cerium oxide (CeO_2) also exists as pellets. These pellets are ideal for the microfurnace calibration because they are high-emissivity, nonreactive, and noncorrosive, and the pellets are similar in size and shape to the mineral and glass samples being analyzed. The pellets can withstand the high temperatures of the microfurnace, and they have no known phase transitions within the temperature range of the furnace. In conjunction with the furnace aperture port, which mimics a blackbody cavity, these pellets provide an acceptable near-blackbody reference material from which an instrument response function and absolute emissivity spectra can be derived from the microfurnace setup.

3.4. Spectral Acquisition

[26] Thermal emission spectra were collected in the Image Visualization and Infrared Spectroscopy (IVIS) Laboratory, at the University of Pittsburgh, using a Nexus 670 spectrometer. Prior to melting glass samples within the microfurnace, it was important to first test a sample with a well-known TIR emissivity spectrum to ensure that the spectra acquired from the microfurnace were accurate and that spectral features

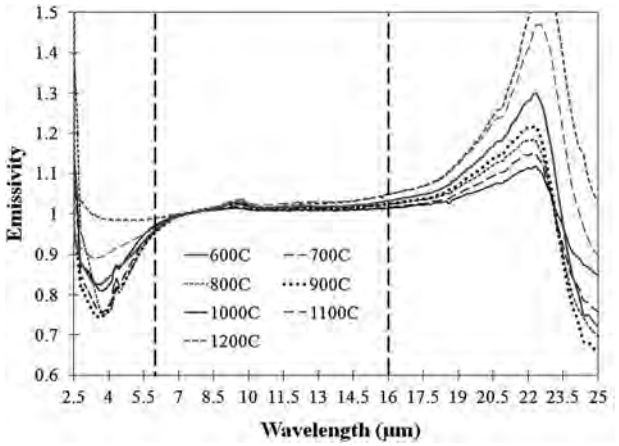

Figure 8. Spectra of cerium oxide pellets within the microfurnace environment from 2.5 to 25 microns, the full wavelength range of the detector. Although the reference spectra do not behave as a perfect blackbody ($\varepsilon = 1$) at all wavelengths, all are relatively featureless (range denoted by vertical dotted lines) between 6 and 16 microns. Shortward of ~6 microns and longward of ~16 microns, the signal-to-noise ratio (SNR) of the detector decreases, and the emissivity becomes nonlinear. All microfurnace spectra are therefore derived within the 6–16 micron range only. This range overlaps with most terrestrial field, airborne and spaceborne TIR sensors and also encompasses the Restrahlen feature of all silicate glasses (~9–11 microns).

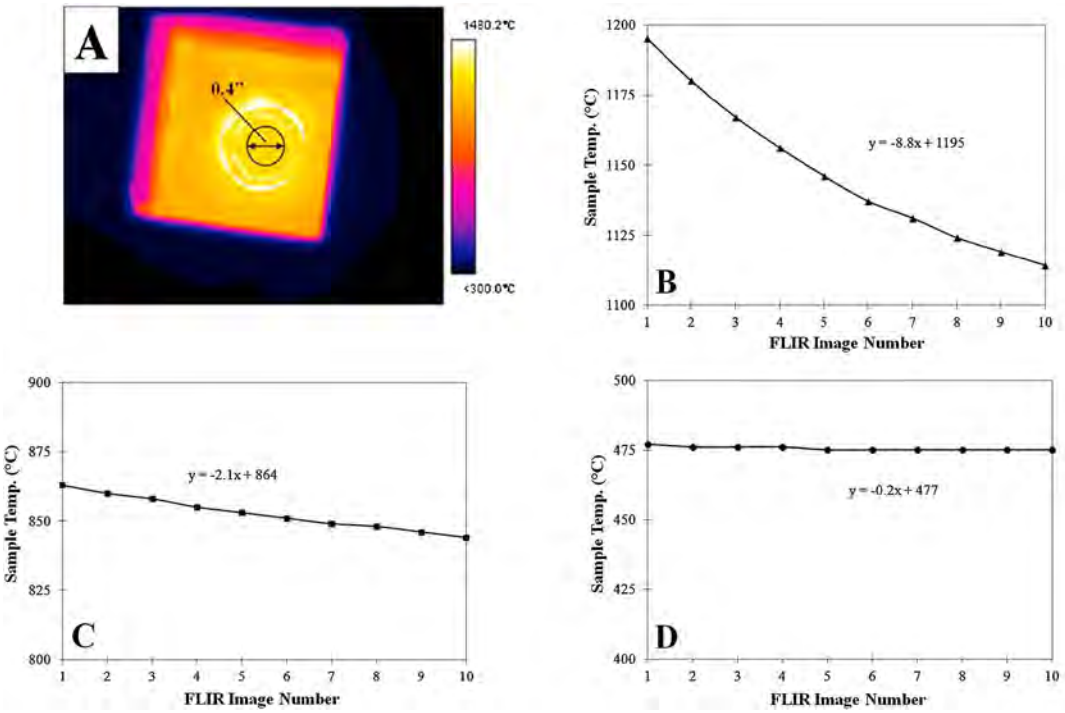

Figure 9. (a) FLIR image of a glass sample in the furnace, taken at a sample temperature of 1500°C. The black 1 cm diameter circle represents the approximate field of view of the spectrometer. Change in the glass sample temperature over a 10 s time period (1 FLIR image/second) is shown for Figure 9a (b) a set point of 1200°C, (c) a set point of 800°C, and (d) a set point of 500°C. The higher the set point, the more sharply the sample temperature decreases over the 10 s time period.

were being properly resolved. Pure quartz sand (SiO_2) was chosen as a first test sample because it has very identifiable spectral features, and it has a melting point higher than the maximum microfurnace set point temperature. The quartz sand was placed into a platinum crucible, and spectra were acquired at 100°C intervals from 1300°C to 500°C. The sample was held at each set point for 5 min before acquisition to ensure that the sample was isothermal.

[27] A synthetic quartzofeldspathic glass ($Ab_{40}An_{14}Q_{46}$) was the first sample to be used to test the melting capacity of the furnace. Approximately 2 g were crushed into millimeter-sized pieces, placed into a platinum crucible, and heated to 1400°C (~200°C above the liquidus). This was done to ensure that all the glass particles were fully melted. Spectra were acquired of the glass in 100°C increments from 1400°C to 500°C. The glass was held for ~5 min at each set point temperature. Because of the extreme TIR signal intensity associated with these temperatures, and the variable and dynamic environmental temperatures within the microfurnace, spectra were acquired/averaged over six scans (~10 s) compared to the 250–1000 scans that are acquired for the standard low temperature setup. Once the sample was fully cooled to room temperature, a low-temperature emissivity spectrum was also acquired for comparisons to previous low-temperature spectra of the same sample, as well as to the high-temperature spectra. Absolute emissivity spectra of the sample at each set point temperature were then derived. The wavelength position and value of the emissivity minimum were then noted for each of the mineral and glass spectra.

3.5. Comparison of Quenched and Slowly Cooled Oligoclase Feldspar

[28] The laboratory emission spectra of crystalline and vitrified oligoclase feldspar were studied by *Ramsey* [1996] in order to determine the spectral changes that occur from a crystalline to a fully glassy physical state. In that earlier study, samples of oligoclase were heated to four different temperatures (80°C, 1130°C, 1220°C, and 1490°C) and quickly cooled. Emissivity spectra of the four samples were then acquired in order to characterize the spectral changes that occurred as the oligoclase transitioned from a completely crystalline material to a completely glassy material (as well as within the two-phase field of oligoclase). The spectral features inherent in crystalline oligoclase began to disappear at ~1200°C and were replaced by the characteristic broad absorption features of a glassy material. At 1490°C, the spectrum of the sample indicated that the sample was completely glassy. However, this study did not make any attempt to measure the samples while at the high temperature.

[29] Emissivity spectra of a similar oligoclase powder (at ~20–80 μm particle size) to that used by *Ramsey* [1996] were acquired in the microfurnace from 1500°C to 500°C to ensure that the sample underwent a complete transition from crystalline mineral to glass. The 1500°C, 1200°C, 1100°C, and 80°C spectra acquired in situ in the IVIS laboratory were then compared to the four quenched glass spectra presented by *Ramsey* [1996]. For ease of comparison, a series of wavelengths was chosen between 7 and 14 μm, and the emission value at each wavelength was used to create plots of each of the spectra.

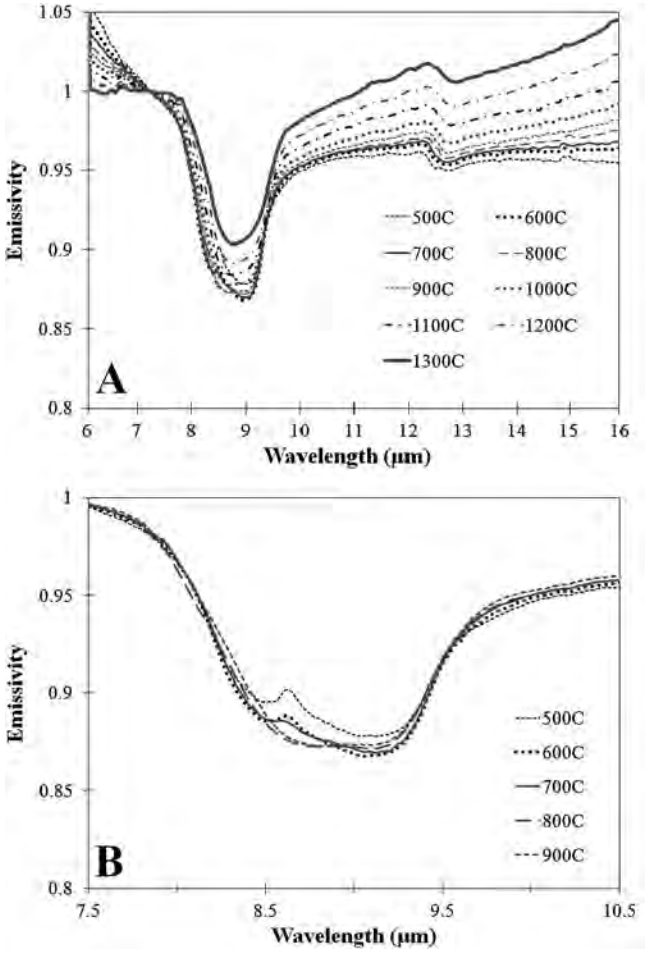

Figure 10. (a) Quartz sand emissivity spectra from 500°C to 1300°C. (b) The doublet feature of quartz between 7.5 and 10.5 microns at temperatures from 500°C to 900°C. The characteristic doublet feature of quartz can be clearly seen in the 500°C and 600°C spectra. At 700°C, the doublet feature significantly shallows, and completely disappears at higher temperatures. This is attributed to the α-to-β quartz phase transition at ~573°C [*Gervais and Piriou*, 1975].

4. Results

4.1. Furnace Testing

[30] The microfurnace port is opened and closed many times during sample spectrum acquisition. Therefore, it was imperative to assess the behavior of the air temperature above the port and determine a maximum time period the port could safely remain open at any given set point. The change in air temperature over a 60 s time period for set points between 500°C and 1200°C is shown in Figure 5a. Set point temperatures up to 900°C remained below the maximum operating temperature of the mirror assembly over the entire 60 s. However, at set point temperatures greater than 900°C, the maximum temperature exceeded at 30 s or less. Therefore, the higher the set point of the furnace, the shorter the amount of time it can remain open during spectrum acquisition without potential damage to the mirror.

[31] It was also important to determine whether any changes in spectral character occur if the port remains open for a given time period prior to spectral acquisition. The quartz sand was heated to a series of set points up to 900°C, and the furnace port was left open for 30 s before acquiring a spectrum. These spectral data were compared to those acquired immediately upon opening the port. For a given set point temperature, no significant difference exists between a quartz spectrum taken immediately and a quartz spectrum taken after 30 s (Figure 5b). This indicates that any changes in air temperature above the furnace port have a minimal effect on the spectra and that change in sample temperature during spectral acquisition is the primary factor affecting spectral morphology.

[32] In order to collect data in a consistent manner and provide an adequate signal-to-noise ratio (SNR) of >1000, it was determined that the furnace only needs to remain open for a maximum of 10 s at all temperatures. The surface-mounted thermocouple placed near the microfurnace port measured the surface temperature of the water-cooled cover every 50°C. Although the cover temperature increased steadily with increasing microfurnace temperature, it did not exceed an outer surface temperature of 35°C, even near the edges of the port. This confirmed the efficiency of the water cooling system in drawing excess heat away from the outer surfaces of the microfurnace and ensured the safety of surrounding equipment and human operators.

[33] Because the heating elements are required to heat the sample to a specific temperature and account for heat losses through the air, the furnace interior, and the power supply, it was expected that the heating element temperature would have to exceed the sample temperature at any given time.

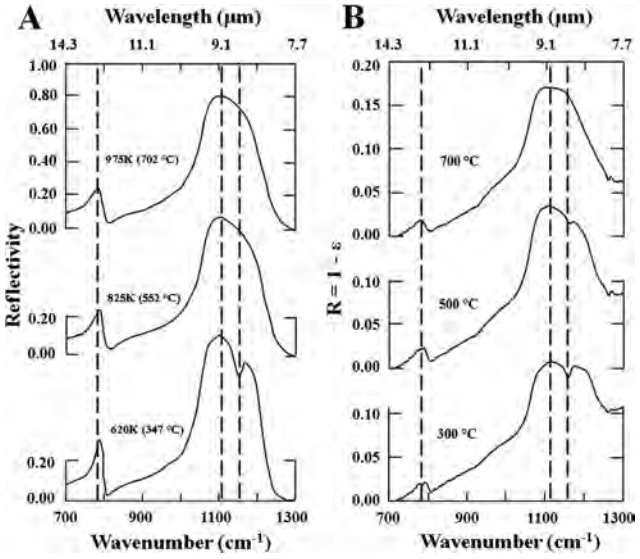

Figure 11. Comparison of quartz reflectivity spectra at three temperatures from (a) *Gervais and Piriou* [1975] and (b) this study. Vertical dotted lines denote the major quartz spectral features. Spectra in this study were converted from emissivity to reflectance using $R = 1 - \varepsilon$. Discrepancies can be attributed to the different spectral acquisition methods between the two studies, as well as a currently unavoidable downwelling radiance component in the furnace imparting greybody energy onto the sample. Despite this, in both studies, the quartz doublet feature at ~9 microns is present in the 300°C spectra and gradually disappears from the spectra as the temperature increases, indicating a phase change in the quartz. At 700°C, the doublet is absent.

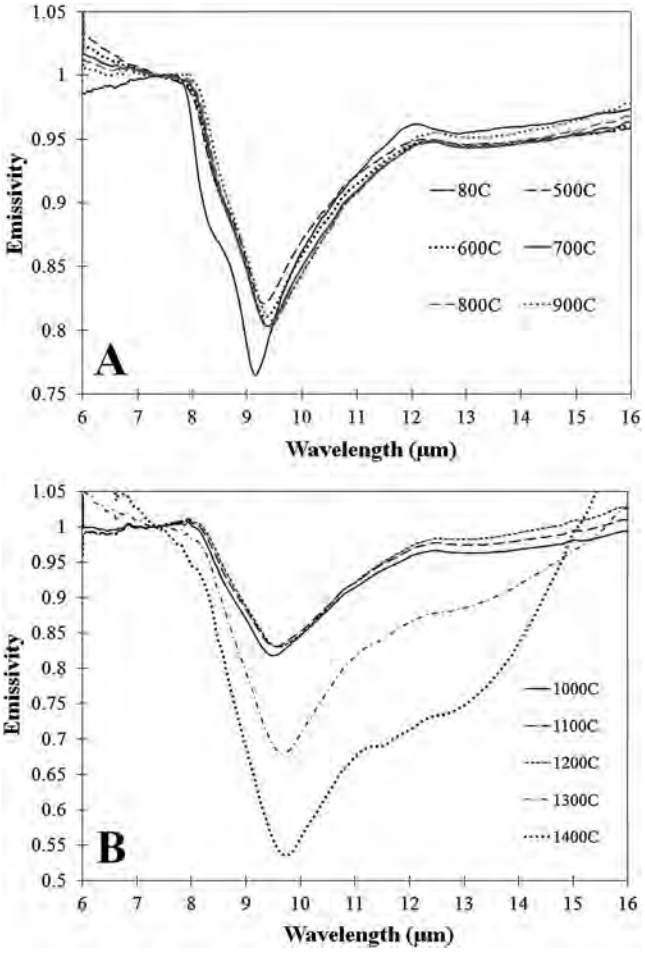

Figure 12. Emissivity spectra of the synthetic glass sample (a) from 80°C (acquired in low-temperature setup) to 900°C and (b) from 1000°C to 1400°C. The spectra show changes in emissivity minimum value and minimum position with increasing temperature. Beyond the liquidus temperature (1250°C), the emissivity minimum values drop sharply. The sharp rise in emissivity of the 1400°C spectrum at ~13 microns is attributed to a large amount of sample intensity interacting with the lower sensitivity of the Deuterated Triglycine Sulfate (DTGS) detector.

Element temperature versus sample temperature was compared for the bare platinum crucible and the crucible with the quartz sand sample (Figure 6a). Whereas heating element temperature remains the same in both cases, the quartz sample and the bare crucible temperatures differ from the element temperature by as much as 250°C. Furthermore, there is a consistently larger difference in temperature between the chamber with a sample compared to the chamber with a bare crucible. This indicates that the difference in temperature between the sample and the heating elements is dependent on the thermal conductivity and thermal inertia of the sample. The calculated difference between sample temperature and heating element temperature for both the bare crucible and the quartz sample shows that the bare crucible has a lower overall temperature difference than the quartz; however, both behave similarly over the range of set point temperatures (Figure 6b).

4.2. Calibration

[34] The intensities of both the cerium oxide pellets and a glass sample at temperatures between 1400°C and 500°C are shown in Figure 7. The overall lower intensity of the cerium oxide compared to the glass sample, combined with a downwelling radiance component within the microfurnace that cannot currently be completely removed, lead to a muting of the microfurnace spectra. Despite this, the overall spectral shapes are still preserved, and changes in the spectra with temperature are resolved. At temperatures greater than 1200°C, a significant rise in intensity occurs at approximately 13 to 17 microns in both the glass and cerium oxide. This increase in intensity is an error due to the decrease in throughput of the detector at these longer wavelengths and also corresponds to a sharp rise in emissivity within the same wavelength region for all samples at high temperatures (Figure 12).

[35] A series of near-blackbody reference spectra were derived from the cerium oxide radiance data (Figure 8). These reference spectra appear relatively featureless between ~6 and 16 microns. The slopes in these spectra, particularly in the 6–8 micron region, can be attributed to slight errors in the calculation of both environmental and sample temperatures [see *Ruff et al.*, 1997] due to the unavoidable dynamic nature of these two temperatures within the furnace environment. These errors also manifest as variable slopes in the glass and mineral emissivity spectra in the 6–8 micron region. The decrease in SNR of the cerium oxide spectra at wavelengths <6 microns and >16 microns currently dictates this as the calibrated spectral range for the microfurnace-derived spectra (Figure 8). Furthermore, this is an acceptable wavelength range for direct comparison with data from current terrestrial field-based, airborne, and spaceborne TIR sensors, which mainly operate in the 8–2 -micron atmospheric window.

4.3. Sample Temperature

[36] Thermal infrared images were collected from glass samples by an FLIR camera at a range of set point temperatures during furnace operation in order to examine the temperature changes and heat loss within the furnace sample chamber. An example image of a glass sample at 1500°C is shown in Figure 9a. The walls of the microfurnace port are somewhat cooler than the glass sample, and areas of much hotter temperatures can be seen around the edges of the sample crucible. This confirms that temperatures within the furnace are somewhat heterogeneous at a given set point, particularly when the furnace port is opened. Figures 9b–9d show the decrease in FLIR-derived sample temperature over a 10 s time period at three set point temperatures. As expected, the higher the set point, the more sharply the sample temperature decreases over the 10 s time period that the furnace port is opened.

4.4. Microfurnace Spectra of Quartz Sand

[37] The series of quartz mineral spectra acquired from the microfurnace are shown in Figure 10a. Although somewhat muted, the characteristic doublet feature of the quartz at 9 microns is clearly resolved in the 500°C spectrum. At 600°C, the doublet becomes less prominent, and at temperatures above 700°C, the doublet feature disappears altogether. This change in spectral shape with temperature is attributed

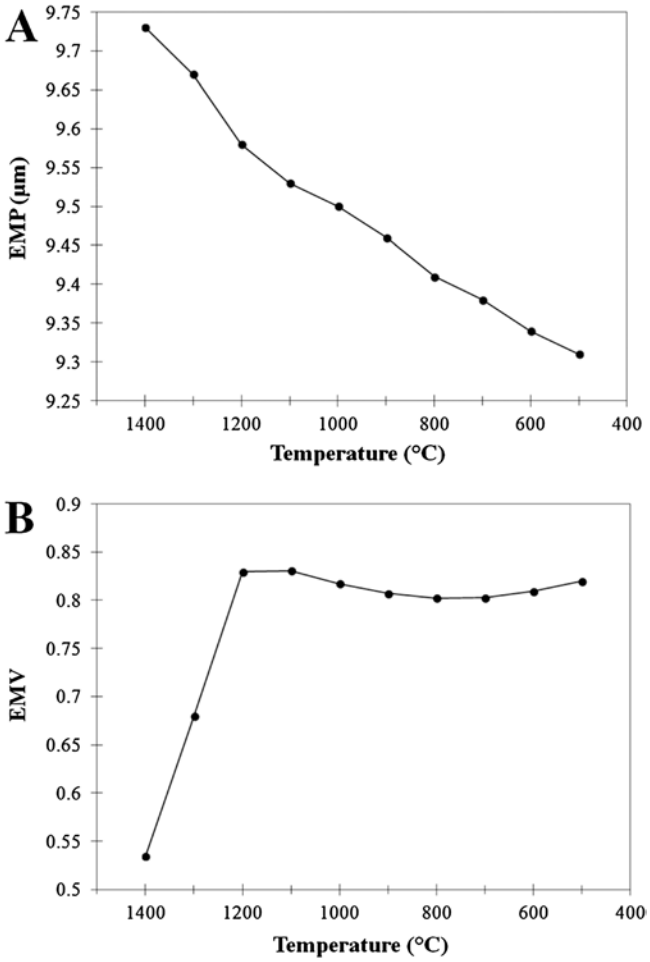

Figure 13. (a) EMP and (b) EMV versus set point temperature for the synthetic glass sample. The EMP decreases steadily with decreasing temperature. EMV rises sharply from 1400°C to 1200°C, indicating the transition from a fully molten material to a more solid material. At temperatures below 1200°C, EMVs decrease more linearly with decreasing temperature.

to the α-to-β phase transition of quartz [*Gervais and Piriou*, 1975]. In order to validate the changes in quartz with temperature, several quartz spectra were compared to quartz infrared reflectivity spectra collected by *Gervais and Piriou* [1975]. Quartz emissivity spectra at three temperatures (300°C, 500°C, and 700°C) were converted into reflectivity ($R = 1 - \varepsilon$), and the spectral morphologies from the two studies were compared (Figure 11). The spectra at each temperature match well in morphology, and the doublet feature behaves similarly in both cases, disappearing from the quartz spectra above at ~700°C. However, discrepancies in reflectivity values exist between the two studies. These are due to differences in both the calibration and data collection methods, as well as the presence of the downwelling radiance component in the microfurnace, which imparts greybody energy onto the sample and mutes the spectral features.

4.5. Synthetic Glass Melt

[38] A synthetic glass sample ($Ab_{40}An_{14}Q_{46}$) was melted in the microfurnace above its calculated liquidus (1250°C) and then cooled. Emissivity spectra were acquired from 1400°C to 500°C (Figure 12). As expected, differences in spectral characteristics are clearly seen with decreasing temperature. Between 1400°C and 1200°C, the emissivity minimum value (EMV) rises sharply and the emissivity minimum position (EMP) shifts toward shorter wavelengths (Figures 12 and 13). The sharp rise in EMV corresponds to structural changes in the bond length/angles as the molten glass cools from 1400°C, approaches its liquidus temperature, and starts to form a solid crust. With decreasing temperature below 1200°C, the EMV changes, and the EMP continues to shift toward shorter wavelengths (Figures 12 and 13).

4.6. Quenched Versus Slowly Cooled Oligoclase Glass

[39] The 1500°C, 1200°C, 1100°C, and 80°C spectra of a powdered oligoclase mineral from the IVIS laboratory were compared to four oligoclase spectra presented in *Ramsey* [1996] (Figure 14). Both of the low temperature (80°C) spectra of the unfused oligoclase demonstrate definitive crystalline spectral features and also match closely with an oligoclase spectrum from the Arizona State University spectral library. The slight differences in emissivity of these

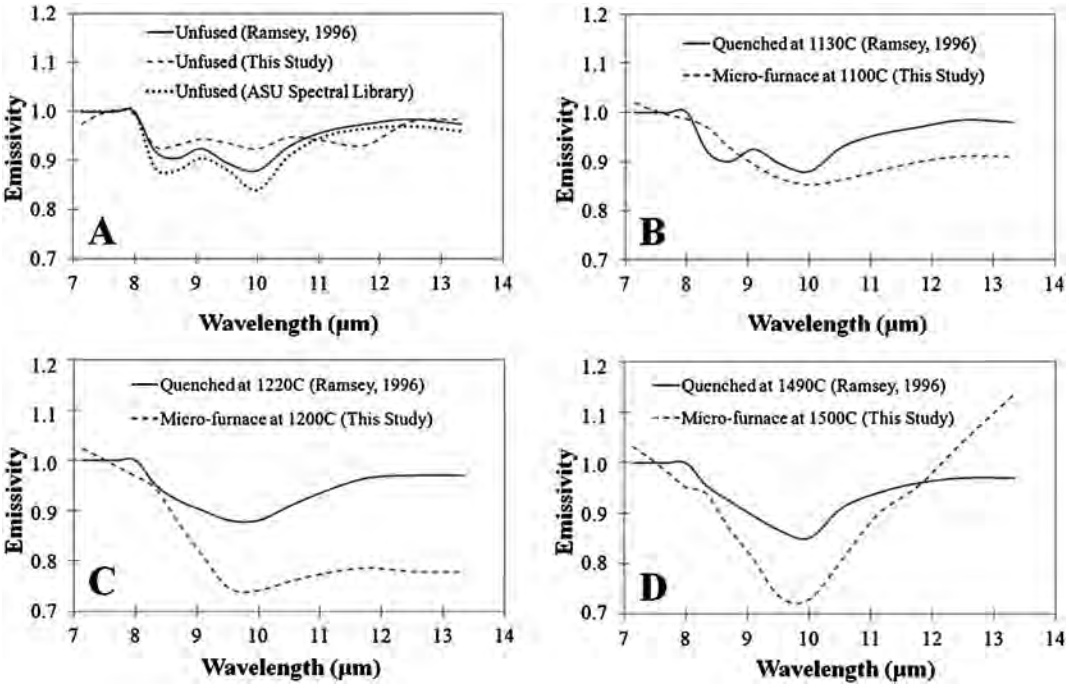

Figure 14. (a) Emissivity spectra of unfused oligoclase feldspar from *Ramsey* [1996], from this study, and from the Arizona State University spectral library. Slight differences in the spectra are due to differences in particle size and small changes in the chemistry of each sample. (b) Emissivity spectrum of oligoclase feldspar quenched at 1130°C *Ramsey* [1996] versus a microfurnace spectrum of oligoclase at 1100°C. (c) Emissivity spectrum of oligoclase feldspar quenched at 1220°C *Ramsey* [1996] versus a microfurnace spectrum of oligoclase at 1200°C. (d) Emissivity spectrum of oligoclase feldspar quenched at 1490°C *Ramsey* [1996] versus a microfurnace spectrum of oligoclase at 1500°C. In Figures 14c and 14d, the EMV of the quenched oligoclase is higher than that of the nonquenched oligoclase melted in the microfurnace.

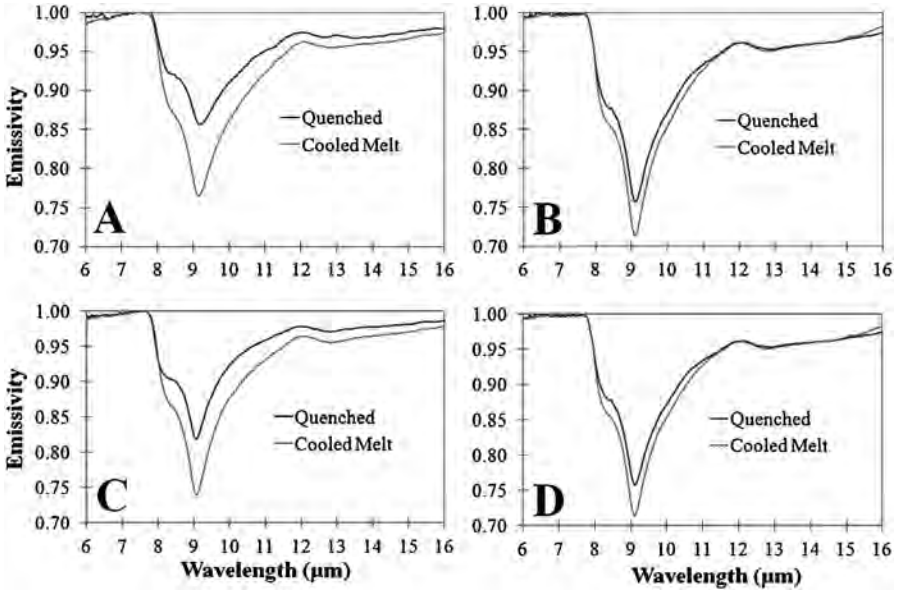

Figure 15. Low temperature (80°C) emissivity spectra of rapidly quenched glass compared to 80°C emissivity spectra of glass slowly cooled to a solid. (a) Glass sample $Ab_{40}An_{14}Q_{46}$ is compared to three other glasses in the synthetic glass suite: (b) glass sample $Ab_{36}An_{12}Q_{51}$, (c) glass sample $Ab_{28}An_{29}Q_{43}$, and (d) glass sample $Ab_{26}An_{10}Q_{64}$. In all cases (including those not shown here), the spectra of rapidly quenched glasses (black lines) have higher emissivity minima than their slowly cooled counterparts (gray lines).

samples can be attributed to the differences in particle size and composition of the oligoclase sample used in each study. At 1220°C and 1490°C, the quenched glass spectra from *Ramsey* [1996], although similar in shape to the microfurnace spectra, display higher emissivity values from 7 to 14 microns than the spectra of samples slowly cooled in the microfurnace. Analysis of the 80°C spectra of quenched versus slowly cooled glass samples showed a similar result, suggesting that the emissivity of a rapidly quenched glass is higher than that of a glass slowly cooled to a solid, and that growth of microlites in the slowly cooled glass could be contributing to the spectral morphology (Figure 15).

5. Discussion

[40] Extensive testing of the microfurnace has shown that it is able to work safely and efficiently within the spectrometer emission setup to acquire TIR data. Thermal heterogeneities that exist within the furnace materials surrounding the sample, as well as within the sample itself, cannot be avoided. Specifically, fluctuations in sample temperature at a given set point currently preclude a time-averaged sample temperature measurement over a long period. However, this error is minimized with the short scan times needed at these high temperatures. It has also been shown that a blackbody environment can be approximated using cerium oxide pellets within the furnace aperture. Significant differences in EMP, EMV, and spectral shapes can be resolved in all spectra with increasing and decreasing temperature, and differences in emissivity exist between quenched and slowly cooled glass samples. These data and results validate the use of thermal emission spectroscopy to study silicate glass and melt structure/petrology in the laboratory.

5.1. Sample Temperature and Calibration

[41] If an object is at a different temperature than its surroundings, heat will transfer from the higher temperature object to the lower temperature object, until thermal equilibrium is reached. At lower set point temperatures, the temperature difference between the heating elements and the sample is large, because the elements heat up significantly faster than the sample. The input of heat is transferred to the surrounding microfurnace insulation via conduction. After approximately 20 min, thermal equilibrium is approached, the temperature difference between the heating elements and the microfurnace insulation is greatly reduced, and the sample begins to stabilize. The difference in temperature between the heating element and sample is also sample-dependent. A larger difference in temperature exists between the quartz sample and the heating elements, as compared to the bare platinum crucible, indicating that the thermal conductivity, and hence the thermal inertia, of the sample itself affects the temperature difference and can also affect the efficiency with which the sample retains heat.

[42] FLIR analysis of the sample and the microfurnace chamber temperatures indicate that the sample temperature changes over the time the port remains open for spectrum acquisition, particularly at higher set point temperatures. This makes an accurate determination of sample temperature difficult. This is a similar (but more extreme) situation to the one that arises in the one temperature method described in *Ruff et al*. [1997] and used for the low-temperature (80°C) spectra presented here. The sample temperature is never measured directly, but rather calculated at a given wavelength in conjunction with a well-known instrument response function. The instrument response function is normally derived from the measurement of two blackbody spectra at very precise temperatures. The variable nature of temperatures in the microfurnace environment necessitated a modification to this one-temperature method, in which the cerium oxide pellets within the furnace chamber were utilized as an approximate blackbody reference. The muting of spectral features that occurs in the microfurnace derived spectra is due to incompletely removed downwelling radiance from the hot walls of the furnace chamber, imparting greybody energy onto the sample. The calibration method currently does not completely remove this effect because it lacks true blackbody measurements at well-constrained temperatures.

[43] The significant rise in signal intensity, coupled with a similar rise in emissivity at higher temperatures (Figure 12), which occurs toward longer wavelengths in all samples, was determined not to be a function of melt, as it also occurs in unmelted quartz mineral spectra. Furthermore, the feature is not associated with any known phase change in either the quartz powder or the glasses. Microprobe and geochemical data of the glasses indicate that each contains a certain percentage of water. Water and water vapor are known to introduce spectral features at given wavelengths in the TIR; however, the rise in intensity is present regardless of the amount of water within the samples, and there does not appear to be a direct correlation between these two parameters.

5.2. Emissivity Spectra of Minerals and Glass

[44] The emissivity spectra of the quartz sand confirm that meaningful spectral features can be resolved using the calibrated microfurnace procedure. Quartz undergoes several reversible phase changes with increasing temperature, and each phase change is accompanied by a change in the symmetry, volume, and shape of the quartz lattice structure [*Le Chatelier*, 1889]. At standard atmospheric pressure and low temperatures, quartz exists in a stable α phase. However, at 573°C, quartz undergoes a transition to hexagonal β quartz. The loss of the doublet feature in the quartz spectra above 700°C suggests that this phase change is complete and detected in the emission spectra. An additional phase change occurs at 870°C, where hexagonal β quartz transitions to tridymite. However, tridymite may not form from pure β quartz. Trace amounts of certain compounds must be added to the quartz in order for the phase transition to take place [*Heaney*, 1994]. The quartz does not display any significant spectral changes between 800°C and 900°C, suggesting that this phase transition likely did not take place. The quartz was not heated to high enough temperatures in this study to detect any spectral changes associated with other phase transitions such as the cubic β cristobalite (1470°C) or quartz melt (1728°C) [*Spearing et al*., 1992].

[45] Differences in spectral characteristics with increasing temperature can also be resolved in the glass melt spectra. The sharp rise in the EMV above the liquidus temperature, and the shift of the minima to shorter wavelengths, suggests that the transition of the glass from a fully molten material, to a two-phase (glass and melt) material, and finally to a

solid material (glass) are being detected in the emissivity spectra. At 1300°C and 1400°C, the spectra indicate that the material is in a fully molten state. Unlike a solid material, which may only have bending and stretching vibrations within its molecular structure, a fully molten material will exhibit several more degrees of freedom in structural movement, thus changing the spectral character of the material. This is manifested in the spectra as a general broadening of the main absorption feature, the appearance of a sharper slope between 6 and 8 microns, and a significant lowering of the depth of the emissivity minimum (Figure 12b).

[46] A comparison of oligoclase feldspar spectra from *Ramsey* [1996] with the spectra of an oligoclase feldspar melt in this study show that the emissivity minimum of a glassy material in a quenched, solid state is systematically higher than a material slowly cooled within the microfurnace. A rapidly quenched melt retains the molecular structure of the temperature at which it was quenched, with almost no microlites forming. Examination of the slowly cooled glasses under a petrographic microscope confirmed that a small amount of microlite growth occurred during cooling within the microfurnace environment. The presence of microlites in large enough amounts can introduce additional spectral features into a glass or melt. However, in this case, the main silicate absorption feature was simply deepened relative to that of the quenched sample. This deepening affects the emissivity minimum value of the glass spectrum.

6. Conclusions

[47] A custom laboratory microfurnace has been successfully developed, calibrated, and tested to acquire emissivity spectra of actively melting and cooling samples. Initial testing has shown that the microfurnace operates effectively and safely within the laboratory and generates significant and meaningful emissivity data of glasses and melts. In the absence of a blackbody detected under the same viewing conditions as the sample, and capable of reaching and sustaining precise temperatures, an alternative calibration method to *Ruff et al*. [1997] has been devised utilizing high-emissivity cerium oxide pellets within the furnace sample chamber as the blackbody reference. This method is currently the most feasible means for deriving absolute emissivity spectra that, although muted due to downwelling energy, still retain the expected spectral morphology and characteristics of the material.

[48] A synthetic glass has been melted within the microfurnace up to 1500°C, and emissivity spectra have been successfully acquired. Additionally, microfurnace spectra have been collected from an oligoclase powder/melt and an unmelted quartz sand sample. All spectra show clear changes in overall morphology with temperature. Furthermore, the onset of the glass melting can be detected in the higher-temperature emissivity spectra due to the changes in the vibrational behavior of the sample, as evidenced by significant changes in the EMV between ~1400°C and 1200°C.

[49] The microfurnace provides the first in situ laboratory thermal emission spectra of glassy melts, allowing for characterization of the spectral morphology of samples as they melt, cool, and form solid crusts. Future work includes documentation of a rhyolitic suite of synthetic glasses as well as expanding the suite to include those of basaltic and andesitic compositions. All of these data will ultimately serve as a well-controlled and calibrated basis for understanding changes in the emissivity spectral features associated with changes in composition, temperature, and rheology of active lava flows and domes. A better understanding of how glassy crusts and micron scale surface textures on cooling lava domes and flows affect emitted energy directly impacts, for example, cooling and flow propagation models that rely on emissivity for the calculation of radiative cooling. If the emissivity of a melt is in fact much lower than the assumed emissivity of solidified glassy lavas, the efficiency of the flow to form a crust and cool, as well as the ultimate flow length, will be affected. The data from these laboratory experiments will also have implications for laboratory petrology and spectroscopy of glasses and melts.

[50] **Acknowledgments.** Funding for this research was made possible through several grants to Ramsey from the Petrology and Geochemistry Program of the National Science Foundation (EAR-1019558, EAR-0711056, and EAR-0309631) as well as from NASA through ASTER Science Team (NNX11AL29G).

References

Abtahi, A. A., A. B. Kahle, E. A. Abbott, A. R. Gillespie, D. Sabol, G. Yamada, and D. Pieri (2002), Emissivity changes in basalt cooling after eruption from Pu'u 'O'o, Kilauea, Hawaii, *Eos Trans. AGU*, Fall Meet. Suppl., Abstract V71A-1263.

Agarwal, A., and M. Tomozawa (1997), Correlation of silica glass properties with the infrared spectra, *J. Non-Cryst. Solids*, *209*, 166–174.

Anderson, S. W., E. R. Stofan, S. E. Smrekar, J. E. Guest, and B. Wood (1999), Pulsed inflation of pahoehoe lava flows: Implications for flood basalt emplacement, *Earth Planet. Sci. Lett.*, *168*, 7–18.

Baloga, S. M., and D. C. Pieri (1986), Time dependent profiles of lava flows, *J. Geophys. Res.*, *91*(9543), 9553.

Bell, R. J., N. F. Bird, and P. Dean (1968), The vibrational spectra of vitreous silica, germania, and beryllium fluoride, *J. Phys. Chem. (Proc. Phys. Soc.)*, *1*, 299–303.

Brown, C. M., R. H. Naber, S. G. Tilford, and M. L. Ginter (1973), High temperature furnace system for vacuum ultraviolet spectroscopic studies, *Appl. Opt. IP*, *12*, 1858.

Byrnes, J. M., D. A. Crown, and M. S. Ramsey (2000), Thermal remote sensing characteristics of basaltic lava flow surface units: Implications for flow field evolution, *Lunar Planet. Sci.* [*CD ROM*], XXXI, abstract #1867.

Byrnes, J. M., M. S. Ramsey, and D. A. Crown (2004), Surface unit characterization of the Mauna Ulu flow field, Kilauea volcano, Hawaii, using integrated field and remote sensing analyses, *J. Volcanol. Geotherm. Res.*, *135*, 169–193.

Byrnes, J. M., P. L. King, M. S. Ramsey, and R. J. Lee (2007), Thermal infrared reflectance and emission spectroscopy of quartzofeldspathic glasses, *Geophys. Res. Lett.*, *34*, L01306, doi:10.1029/2006GL027893.

Carter, A. J., M. S. Ramsey, and A. B. Belousov (2007), Recent crater formation at Bezymianny Volcano lava dome: Significant changes observed in satellite and field data, *Bull. Volcanol.*, *69*, 811–815, doi:10.1007/s00445-007-0113-X.

Clark, R. N. (1999), Spectroscopy of rocks and minerals, and principles of spectroscopy in *Manual of Remote Sensing, Volume 3, Remote Sensing for the Earth Sciences*, edited by A. N. Rencz, pp. 3–58, John Wiley, New York.

Crisp, J., and S. Baloga (1990), A model for lava flows with two thermal components, *J. Geophys. Res.*, *95*, 1255–1270.

Crisp, J., and S. Baloga (1994), Influence of crystallization and entrainment of cooler material on the emplacement of basaltic a'a lava flows, *J. Geophys. Res.*, *99*, 11819–11831.

Crisp, J., A. B. Kahle, and E. A. Abbot (1990), Thermal infrared spectral character of Hawaiian basaltic glasses, *J. Geophys. Res.*, *95*(B13), 21657–21669.

Dalby, K. N., and P. L. King (2006), A new approach to determine and quantify structural units in silicate glasses using micro Fourier-Transform Infrared spectroscopy, *Am. Mineral.*, *91*, 1783–1793, doi:10.2138/am.2006.2075.

Dalby, K. N., C. D. M. Dufresne, P. L. King, J. M. Byrnes, R. J. Lee, and M. S. Ramsey (2006), Characterization of glasses using infrared spectroscopy, *Geochim. Cosmochim. Acta Suppl.*, *70*(18), 125.

Daniel, I., P. H. Gillet, P. F. McMillan, and P. Richet (1995), An in-situ high temperature study of stable and meta-stable CaA12Si20 8 - polymorphs, *Mineral. Mag.*, *59*, 25–34.

Domine, F., and B. Piriou (1983), Study of sodium silicate melt and glass by infrared reflectance spectroscopy, *J. Non-Crystal. Solids*, *5*, 125–130.

Dowty, E. (1987), Vibrational interactions of tetrahedral in silicate glasses and crystals: 1. Calculations on ideal silicate-aluminate-germanate structural units, *Phys. Chem. Miner.*, *14*, 80–93.

Dufresne, C. D. M., P. L. King, M. Darby Dyar, and K. N. Dalby (2009), Effect of SiO_2, total FeO, Fe^{3+}/Fe^{2+}, and alkali elements in basaltic glasses on mid-infrared spectra, *Am. Mineral.*, *94*, 1580–1590.

Farges, F., and G. E. Jr.Brown (1996), An empirical model for the anharmonic analysis of high-temperature XAFS spectra of oxide compounds with applications to the coordination environment of Ni in NiO, γ-Ni2SiO4 and Ni-bearing Na-disilicate glass and melt, *Chem. Geol.*, *128*, 93–106.

Farnan, I., and J. F. Stebbins (1990), High-temperature 298i NMR investigation of solid and molten silicates, *J. Am. Chem. Soc.*, *112*, 32–39.

Gervais, F., and B. Piriou (1975), Temperature dependence of transverse and longitudinal optic modes in the α and β phases of quartz, *Phys. Rev. Lett.*, *11*, 3944–3950, doi:10.1103/PhysRevB.11.3944.

Grove, J., and P. E. Jellyman (1955), The infrared transmission of glass in the range room temperature to 1400°C, *J. Soc. Glass Technol.*, *39*, 3.

Gruener, G., P. Odier, D. DeSousa Meneses, P. Florian, and P. Richet (2001), Bulk and local dynamics in glass-forming liquids: a viscosity, electrical conductivity, and NMR study of aluminosilicate melts, *Phys. Rev. B*, *64*, 24206.

Grzechnik, A., and P. F. McMillan (1998), Temperature dependence of the OH^- absorption in SiO_2 glass and melt to 1975 K, *Am. Mineral.*, *83*, 331–338.

Harris, A. J. L., and S. Rowland (2001), FLOWGO: a kinematic thermo-rheological model for lava flowing in a channel, *Bull. Volcanol.*, *63*, 20–44.

Harris, A. J. L., L. P. Flynn, L. Keszthelyi, P. J. Mouginis-Mark, S. K. Rowland, and J. A. Resing (1998), Calculation of lava effusion rates from Landsat TM data, *Bull. Volcanol.*, *60*, 52–71.

Harris, A. J. L., J. Dehn, M. Patrick, S. Calvari, M. Ripepe, and L. Lodato (2006), Lava effusion rates from hand-held thermal infrared imagery: an example from the June 2003 effusive activity at Stromboli, *Bull. Volcanol.*, *68*, 107–117, doi:10.1007/s00445-005-0425-7.

Heaney, P. J. (1994), Structure and chemistry of the low-pressure silica polymorphs, in *Reviews in Mineralogy, Silica-Physical Behavior, Geochemistry and Materials Applications*, *29*, Mineralogical Society of America, Washington, D. C.

Helgason, H., P. Gunnlaugsson, K. Jonsson, and S. Steinthorsson (1994), High temperature Mossbauer spectroscopy of titanomagnetite and maghemite in basalts, *Hyperfine Interact.*, *91*, 595–599.

Ildefonse, P., D. Cabaret, P. H. Sainctavit, G. Calas, A.-M. Flanck, and P. Lagarde (1998), Aluminum X-ray absorption near edge structure in model compounds and Earth's surface minerals, *Phys. Chem. Miner.*, *25*, 112–121.

Keszthelyi, L., and R. Denlinger (1996), The initial cooling of pahoehoe flow lobes, *Bull. Volcanol.*, *58*, 5–18.

King, P. L., M. S. Ramsey, P. F. McMillan, and G. Swayze (2004), Laboratory Fourier transform infrared spectroscopy methods for geologic samples, in *Infrared Spectroscopy in Geochemistry, Exploration Geochemistry, and Remote Sensing*, Mineral. Assoc. of Can. Short Course Ser., *33*, edited by P. L. King, M. S. Ramsey, and G. A. Swayze, pp. 57–91, Mineralogical Association of Canada, Ottawa.

King, P. L., C. D. M. Dufresne, and K. N. Dalby (2008), Effect of SiO2, total FeO, Fe^{2+}/Fe^{3+} and alkalis in glasses on thermal infrared spectra, *Lunar Planet. Sci*. [*CD ROM*], *XXXIX*, abstract 2256.

Kirkpatrick R. J. (1988), MAS NMR spectroscopy of minerals and glasses, in *Spectroscopic Methods in Mineralogy and Geochemistry, Reviews in Mineralogy*, *18*, edited by F. C. Hawthorne, pp. 341–403, Mineralogical Society of America, Washington D.C.

Le Chatelier, H. (1889), Sur la dilatation du quartz, *Comptes Rendus*, *108*, 1046.

Lee, R. J., P. L. King, and M. S. Ramsey (2010), Spectral analysis of synthetic quartzofeldspathic glasses using laboratory thermal infrared spectroscopy, *J. Geophys. Res.*, *115*, B06202, doi:10.1029/2009JB006672.

Magnien, V., D. R. Neuville, L. Cormier, B. O. Mysen, V. Briois, S. Belin, O. Pinet, and P. Richet (2004), Kinetics of iron oxidation in silicate melts: a preliminary XANES study, *Chem. Geol.*, *213*, 253–263.

Magnien, V., D. R. Neuville, L. Cormier, J. Roux, J.-L. Hazemann, O. Pinet, and P. Richet (2006), Kinetics of iron redox reactions in silicate liquids: a high-temperature X-ray absorption and Raman spectroscopy study, *J. Nucl. Mater.*, *352*, 190–195.

Malin, M. C. (1980), Lengths of Hawaiian lava flows, *Geology*, *8*, 306–308.

McMillan, P. (1984), Structural studies of silicate glasses and melts—Applications and limitations of Raman spectroscopy, *Am. Mineral.*, *69*, 622–644.

McMillan, P. F., and G. H. Wolf (1995), Vibrational spectroscopy of silicate liquids, in *Structure, Dynamics and Properties of Silicate Melts, Min. Soc. Am. Rev. Mineral*, vol. *33*, edited by J. F. Stebbins, et al., pp. 247–315, Mineralogical Society of America, Blacksburg, Va.

McMillan, P. F., G. H. Wolf, and B. T. Poe (1992), Vibrational spectroscopy of silicate liquids and glasses, *Chem. Geol.*, *96*, 351–366.

McMillan, P. F., B. T. Poe, P. Gillet, and B. Reynard (1994), A study of SiO2 glasses and supercooled liquid to 1950 K via high-temperature Raman spectroscopy, *Geochim. Cosmochim. Acta*, *58*, 3653–3664.

McMillan, P. F., A. Grzechnik, and H. Chotalla (1998), Structural characterization of $SiO_2 \pm CsAlO_2$ and $SiO_2 \pm RbAlO_2$ glasses, *J. Non-Crystal. Solids*, *226*, 239–248.

Minitti, M. E., C. M. Weitz, M. D. Lane, and J. L. Bishop (2007), Morphology, chemistry, and spectral properties of Hawaiian rock coatings and implications for Mars, *J. Geophys. Res.*, *112*, E05015, doi:10.1029/2006JE002839.

Moulton, B. J. A., M. Kanzaki, H. Fukui, N. Hiraoka, and G. S. Henderson (2012), *In situ* high pressure changes to the O *K*-edge electronic structure of CaMgSi2O6: An x-ray Raman approach, *Goldschmidt Conference*, Abstract #1569.

Mysen B. O. (1988), *Structure and Properties of Silicate Melts*, 368 pp., Elsevier, Amsterdam, The Netherlands.

Mysen, B. O. (1990), Role of Al in depolymerized, peralkaline aluminosilicate melts in the systems Li_2O-A1$_2O_3$-SiO_2, Na*O-A1$_2O_9$-SiOZ and K_2O-A1&SiO_2, *Am. Mineral.*, *75*, 120–134.

Mysen, B. O., and J. D. Frantz (1992), Raman spectroscopy of silicate melts at magmatic temperatures: Na_2O-SiOz, K/O-SiOz and Li_2O-SiO_2 binary compositions in the temperature range 25 1475~C, *Chem. Geol.*, *96*, 321–332.

Mysen, B. O., and J. D. Frantz (1993), Structure and properties of alkali silicate melts at magmatic temperatures, *Eur. J. Mineral.*, *5*, 393–407.

Mysen, B. O., D. Virgo, and C. M. Scarfe (1980), Relations between the anionic structure and viscosity of silicate melts—A Raman spectroscopic study, *Am. Mineral.*, *65*, 690–710.

Mysen, B. O., D. Virgo, and L. Kushiro (1981), The structural role of aluminum in silicate melts—A Raman spectroscopic study at I atmosphere, *Am. Mineral.*, *66*, 678–701.

Mysen, B. O., D. Virgo, and F. A. Seifert (1982), The structure of silicate melts: implications for chemical and physical properties of natural magma, *Rev. Geophys. Space Phys.*, *20*, 353–383.

Neuville, D. R., and B. O. Mysen (1996), Role of aluminum in the silicate network: In situ, high-temperature study of glasses and melts on the join SiO_2-$NaAlO_2$, *Geochim. Cosmochim. Acta*, *60*, 1727–1737.

Neuville, D. R., L. Cormier, and D. Massiot (2004a), Al environment in tectosilicate and peraluminous glasses: A 27Al MQ-MAS NMR, Raman, and XANES investigation, *Geochim. Cosmochim. Acta*, *68*, 5071–5079.

Neuville, D. R., L. Cormier, A.-M. Flank, V. Briois, and D. Massiot (2004b), Al speciation and Ca environment in calcium aluminosilicate glasses and crystals by Al and Ca K-edge X-ray absorption spectroscopy, *Chem. Geol.*, *213*, 153–163.

Neuville, D. R., L. Cormier, and D. Massiot (2004c), Al environment in tectosilicate and peraluminous glasses: a 27Al MQ-MAS NMR, Raman, and EXAFS investigation, *Geochim. Cosmochim. Acta*, *68*, 5071–5079.

Neuville, D. R., L. Cormier, and D. Massiot (2006), Al coordination and speciation in calcium aluminosilicate glasses: Effects of composition determined by 27 Al MQ-MAS NMR and Raman spectroscopy, *Chem. Geol.*, *229*, 173–185.

Neuville, D. R., L. Cormier, D. de Ligny, J. Roux, A.-M. Flank, and P. Lagarde (2008), Environments around Al, Si, and Ca in aluminate and aluminosilicate melts by X-ray absorption spectroscopy at high temperature, *Am. Mineral.*, *93*, 228–234, doi:10.2138/am.2008.2646.

Ondrusek, J., P. R. Christensen, and J. H. Fink (1993), Mapping the distribution of vesicular textures on silicic lavas using the thermal infrared multispectral scanner, *J. Geophys. Res.*, *98*, 15,903–15,908.

Pieri, D. C., and S. M. Baloga (1986), Eruption rate, area and length relationships for some Hawaiian lava flows, *J. Volcanol. Geotherm. Res.*, *30*, 29–45.

Pieri, D. C., L. S. Glaze, and M. J. Abrams (1990), Thermal radiance observations of an active lava flow during the June 1984 eruption of Mount Etna, *Geology*, *18*, 1018–1022.

Poe, B. T., P. F. McMillan, C. A. Angell, and R. K. Sato (1992a), Al and Si coordination in SiO_2-Al_2O_3 glasses and liquids: a study by NMR and IR spectroscopy and MD simulations, *Chem. Geol.*, *96*, 333–349.

Poe, B. T., P. F. McMillan, B. Coté, D. Massiot, and J. P. Coutures (1992b), SiO2-A12O3 liquids: in-situ study by high temperature ^{27}A1 NMR spectroscopy and molecular dynamics simulations, *J. Phys. Chem.*, *96*, 8220–8224.

Poe, B. T., P. F. McMillan, B. Coté, D. Massiot, and J. P. Coutures (1993), Magnesium and calcium aluminate liquids: In situ high temperature 27Al NMR spectroscopy, *Science*, *259*, 786–788.

Poe, B. T., P. F. McMillan, B. Coté, D. Massiot, and J. P. Coutures (1994), Structure and dynamics in calcium aluminate liquids: High-temperature 27Al NMR and Raman spectroscopy, *J. Am. Ceram. Soc.*, *77*, 1832–1838.

Poe, B. T., C. Romano, N. Zotov, G. Cibin, and A. Marcelli (2001), Compression mechanisms in aluminosilicate melts: Raman and XANES spectroscopy of glasses quenched from pressures up to 10 GPa, *Chem. Geol.*, *174*, 21–31.

Ramsey, M. S. (1996), Quantitative analysis of geological surfaces: A deconvolution algorithm for midinfrared remote sensing data, Ph.D. dissertation, 276 pp., Ariz. State Univ., Tempe, Ariz.

Ramsey, M. S., and J. Dehn (2004), Spaceborne observations of the 2000 Bezymianny, Kamchatka eruption: the integration of high-resolution ASTER data into near real-time monitoring using AVHRR, *J. Volcanol. Geotherm. Res.*, *135*, 127–146.

Ramsey, M. S. and J. H. Fink (1996), Estimating lava vesicularity: A new technique using thermal infrared remote sensing data, *Eos Trans. AGU*, *77*, Fall Meet. Suppl., p. F803.

Ramsey, M. S. and J. H. Fink (1997), Mapping vesicularity of Hawaiian lava flows via thermal infrared remote sensing, *Eos Trans. AGU*, *78*, Fall Meet. Suppl., p. F777.

Ramsey, M. S., and J. H. Fink (1999), Estimating silicic lava vesicularity with thermal remote sensing: A new technique for volcanic mapping and monitoring, *Bull. Volcanol.*, *61*, 32–39.

Ramsey, M. S. and R. L. Wessels (2007), Monitoring changing eruption styles of Kilauea Volcano over the summer of 2007 with spaceborne infrared data, *Eos Trans. AGU*, *88*(*52*): *Fall Meet. Suppl.*, *Abstract V51H-07*.

Ramsey, M. S., R. J. Lee and A. M. Harburger (2012), Thermal emission from molten silicates: Implications for lava flow emplacement and hazards, *Chapman Conference*: *Hawaiian Volcanoes*, Waikoloa, HI.

Richet, P., P. Gillet, A. Pierre, A. Bouhifd, I. Daniel, and G. Fiquet (1993), Raman spectroscopy, X-ray diffraction, and phase relationship determinations with a versatile heating cell for measurements up to 3600 K (or 2700 K in air), *J. Appl. Phys.*, *74*, 5451–5456.

Ruff, S. W., P. R. Christensen, P. W. Barbera, and D. L. Anderson (1997), Quantitative thermal emission spectroscopy of minerals: A laboratory technique for measurement and calibration, *J. Geophys. Res.*, *102*, 14899–14913.

Salisbury, J. W., L. S. Walter, N. Vergo, and D. M. D'Aria (1991), *Infrared (2.1–25 um) Spectra of Minerals*, Johns Hopkins Univ. Press, Baltimore, MD, pp. 267.

Seifert, F. A., B. O. Mysen, and D. Virgo (1981), Structural similarity between glasses and melts relevant to petrological processes, *Geochim. Cosmochim. Acta*, *45*, 1879–1884.

Seifert, F. A., B. O. Mysen, and D. Virgo (1982), Three-dimensional network structure of quenched melts (glass) in the system SiO2-NaAlO2, SiO2-$CaAl_2O_4$ and SiO_2-$MgAl_2O_4$, *Am. Mineral.*, *67*, 696–717.

Sonneville, C., D. De Ligney, D. R. Neuville, P. Florian, S. Le Floch, C. Le Losq, and G. S. Henderson (2012), Structural modifications in densified soda aluminosilicate glasses, *Goldschmidt Conference*, Abstract #1841.

Spearing, D. R., I. Farnan, and J. F. Stebbins (1992), Dynamics of the alpha-beta phase transitions in quartz and cristobalite as observed by in-situ high temperature ^{29}Si and ^{17}O NMR, *Phys. Chem. Miner.*, *19*, 307–321.

Stebbins, J. F. (1988), Effects of temperature and composition on silicate glass structure and dynamics: Si-29 NMR results, *J. Non-Cryst. Solids*, *106*(359), 369.

Stebbins, J. F., and I. Farnan (1992), Effects of high temperature on silicate liquid structure; a multinuclear NMR study, *Science*, *255*, 586–589.

Stebbins, J. F., and Z. Xu (1997), NMR evidence for excess non-bridging O atoms in an aluminosilicate glass, *Nature*, *390*, 60–62.

Stebbins, J. F., I. Farnan, and X. Xue (1992), The structure and dynamics of alkali silicate liquids: a view from NMR spectroscopy, *Chem. Geol.*, *96*, 371–385.

Vaughan, R. G., R. Wessels, and M. S. Ramsey (2005), Monitoring renewed volcanic activity at Mount St. Helens with high-resolution thermal infrared data: ASTER, MASTER and FLIR, *Eos Trans. AGU*, *86*(52), Fall Meet. Suppl., Abstract V53D-1603.

Vicari, A., A. Ciraudo, C. Del Negro, A. Herault, and L. Fortuna (2009), Lava flow simulations using discharge rates from thermal infrared satellite imagery during the 2006 Etna eruption, *Nat. Hazards.*, *50*, 539–550, doi:10.1007/s11069-008-9306-7.

Woodriff, R., and G. Ramelow (1968), Atomic absorption spectroscopy with a high-temperature furnace, *Spectrochim. Acta*, *23b*, 685–671.

Wright, S. P. and M. S. Ramsey (2006), Thermal infrared data analyses of Meteor Crater, Arizona: Implications for Mars spaceborne data from the Thermal Emission Imaging System, *J. Geophys. Res.*, *111*, E02004, doi:10.1029/2005JE002472.

Wyatt, M. B., V. E. Hamilton, H. Y. Jr.McSween, and P. R. Christensen (2001), Analysis of terrestrial and Martian volcanic compositions using thermal emission spectroscopy: I. Determination of mineralogy, chemistry, and classification strategies, *J. Geophys. Res.*, *106*, 14711–14732.